

## Effect of electrical current pulses on domain walls in Pt/Co/Pt nanotracks with out-of-plane anisotropy: Spin transfer torque versus Joule heating

M. Cormier,<sup>1,2,\*</sup> A. Mougin,<sup>1</sup> J. Ferré,<sup>1</sup> A. Thiaville,<sup>1</sup> N. Charpentier,<sup>1</sup> F. Piéchon,<sup>1</sup> R. Weil,<sup>1</sup> V. Baltz,<sup>3</sup> and B. Rodmacq<sup>3</sup>

<sup>1</sup>Laboratoire de Physique des Solides, Univ. Paris-Sud, CNRS, UMR 8502, F-91405 Orsay Cedex, France

<sup>2</sup>ALTIS Semiconductor, 224 Bd John Kennedy, F-91105 Corbeil-Essonnes Cedex, France

<sup>3</sup>SPINTEC, UMR 8191 CEA/CNRS/UJF/Grenoble INP, INAC, 17 rue des Martyrs, F-38054 Grenoble Cedex, France

(Received 13 October 2009; published 19 January 2010)

The effect of electrical current pulses on magnetic domain walls is studied in a nanometer-scale magnetic track defined in a He<sup>+</sup>-irradiated Pt/Co(0.5 nm)/Pt film with out-of-plane anisotropy. Current pulses in a wide range of intensities and durations are shown to result either in track demagnetization, or in polarity-independent domain-wall propagation, due to Joule heating during the current pulse. None of the expected spin transfer effects is shown to occur. To explain this, the spin-dependent current-density distribution in the stack is evaluated, in the frame of an adapted Fuchs-Sondheimer model. The spin-polarized current density in the cobalt layer is shown to be unexpectedly low as compared to the charge current in the whole stack, which causes Joule heating. This is explained by a low electron transmission at Co/Pt interfaces, as is deduced from resistance measurements on a series of samples with different cobalt thicknesses. This leads us to emphasize that the balance between spin and total charge current densities should be carefully considered when addressing spin transfer torque effects.

DOI: [10.1103/PhysRevB.81.024407](https://doi.org/10.1103/PhysRevB.81.024407)

PACS number(s): 75.60.Ch, 73.63.-b, 72.25.Ba, 85.75.-d

### I. INTRODUCTION

Current developments of magnetic data storage and data processing technologies make highly desirable to control magnetic domain-wall propagation in narrow magnetic tracks.<sup>1-3</sup> In particular, spin transfer torque exerted by a spin-polarized current on a domain wall propagating in a nanotrack is expected to allow a selective and direct addressing of the magnetic configuration of the nanotrack.<sup>4-12</sup> For this purpose, nanotracks defined in ultrathin magnetic films with out-of-plane magnetic anisotropy gather several advantages.<sup>13,14</sup> Indeed, domain walls in these systems are thin,<sup>15,16</sup> which is deemed to enhance the role of the non-adiabatic, field similar, directly efficient spin transfer torque term.<sup>17-19</sup> Moreover, confinement effects due to the low film thickness lead to a lowered Walker breakdown,<sup>13,14,19</sup> which allows to access the so-called precessional domain-wall propagation regime under a reduced field or current excitation; in this regime, both spin transfer torque terms—adiabatic and nonadiabatic—are supposed to be efficient,<sup>19</sup> and the continuous evolution of the domain-wall micromagnetic structure during precessional propagation is expected to lead to a reduced likeliness of the wall to get pinned by the sample's intrinsic or extrinsic defects. This being said, domain-wall pinning still seems to play a predominant role in most of the out-of-plane magnetized metallic systems where current-induced domain-wall motion was observed up to now.<sup>20-25</sup> In this context, a model system with artificially reduced domain-wall pinning is of particular interest so as to get a further insight into the intrinsic processes of current-induced domain-wall depinning and propagation, which are still currently under debate.<sup>26,27</sup>

In this paper, we report (Sec. II) on our experimental study of the effects of electrical current pulses on domain walls, in a magnetic nanotrack defined in an ultrathin Pt/Co/Pt film with out-of-plane magnetic anisotropy, where pin-

ning has been reduced thanks to He<sup>+</sup> irradiation.<sup>28</sup> We show that current pulses in a wide range of intensities, and with durations varying on 3 orders of magnitude, result either in a demagnetized state in the nanotrack or in domain-wall propagation, both unrelated to the pulse polarity. This rules out spin transfer torque effects and is explained by Joule heating due to the current circulation in the track.<sup>20,29-33</sup> To explain the absence of a visible effect of spin transfer torque, spin-polarized electron transport in the cobalt layer of the track is evaluated (Sec. III), and is shown to be in an unfavorable balance with Joule heating. This leads us to update the required conditions for an optimized system for spin transfer torque and to comment on recent results on this topic (Sec. IV).<sup>20-25</sup> Even if this work is focused on out-of-plane magnetized systems, our approach for evaluating spin-polarized current densities in thin metallic layers and our conclusions are more general. They can be applied as well to in-plane magnetized systems, where current-induced domain-wall propagation was first evidenced.<sup>7-9</sup>

### II. EXPERIMENTS

Magnetic nanotracks were patterned in a Pt(4.5 nm)/Co(0.5 nm)/Pt(3.5 nm) film, sputter deposited onto a thermally oxidized Si/SiO<sub>2</sub>(500 nm) substrate. This system presents a strong, interface-induced out-of-plane magnetic anisotropy (7.1 kOe anisotropy field), and is known to reverse its magnetization by few domain nucleations, and predominant easy domain-wall propagation.<sup>16</sup> Before patterning, this film was uniformly irradiated with light He<sup>+</sup> ions, at a very low dose of  $5 \times 10^{15}$  He<sup>+</sup> cm<sup>-2</sup>, with an energy of 30 keV. This irradiation results in a strong reduction in the out-of-plane magnetic anisotropy,<sup>28,34</sup> down to 1 kOe, and consequently in the coercive and domain-wall propagation fields. Domain walls can then propagate under a lower magnetic field (only 1 Oe dc at room temperature),<sup>35</sup> with an

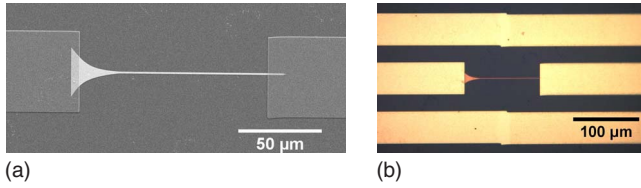


FIG. 1. (Color online) (a) Scanning electron microscopy picture of a patterned Pt/Co/Pt nanotrack. Its trumpetlike nucleation pad is visible at its left end, as well as aluminum contact pads at both ends. (b) Optical microscopy picture of the complete measurement device. The track is visible in the center, surrounded by the aluminum, 50 Ω-matched coplanar line, which allows electrical connection to the pulse generator.

even lower sensitivity to intrinsic and extrinsic pinning. Propagation velocities are thus considerably enhanced.<sup>34–37</sup> Besides, the Curie temperature,  $T_C$ , of the material is reduced from 415 to 365 K.<sup>28,34,35</sup>

The width of the tracks, patterned by a conventional process of e-beam lithography and ion-beam etching through a gold mask, was measured by scanning electron microscopy. For the track described in the following [Fig. 1(a)], it is  $w = 750$  nm, for a typical length of 130 μm. At one end of the track, a trumpetlike enlargement was designed so as to enhance the domain nucleation probability, whereas the other end of the track was designed with a pointed shape. Around the track, a micrometric aluminum 50 Ω-matched coplanar line was designed [Fig. 1(b)], also by e-beam lithography, which allows to make electrical contacts between the track ends and micrometric high-frequency Picoprobes®,<sup>38</sup> directly connected to a voltage-pulse generator. The resistance of the track itself,  $R$ , is close to 0.6 kΩ.<sup>39</sup> However, the resulting impedance mismatch is localized on a 130 μm circuit length, which allows to inject nanosecond-scale pulses without any major degradation of the pulse shape. The cur-

rent density in the track’s cobalt layer during a current pulse is estimated to be on the order of a few  $10^{11}$  A m<sup>-2</sup> per applied volt, as calculated when assuming a uniform current distribution over the track section.

The magnetic measurements, by magneto-optical polar Kerr microscopy at room temperature,  $T_{amb}$ , were performed as follows: first, the sample was magnetically saturated by a strong magnetic field pulse, and a reference magneto-optical image (s) was registered; then, a small field pulse of opposite sign was applied to nucleate a domain in the track, and a second image (n) was taken; finally, the current pulse (or sequence of well-separated current pulses) was injected into the track, at zero applied field, and a third image (p) was taken. The (n)-(s) and (p)-(s) difference images, respectively, show the magnetic configuration in the track before and after current injection, which can thus be compared.<sup>40</sup>

Depending on the applied pulse voltage amplitude,  $U$ , and duration,  $\Delta t$ , three characteristic situations can be observed, regarding the magnetic domain structure in the track (Fig. 2). First, the domain structure is not modified by short and/or low-voltage pulses [Fig. 2(a)]; second, long and/or intense pulses result in a characteristic alternance of small up and down domains [Fig. 2(b)]; finally, for a very narrow range of pulse durations and intensities, current-pulse-induced propagation of the existing domain walls can be observed in some cases [Fig. 2(c)]. The type of the effect observed after the application of a definite pulse in the track is qualitatively reproducible: each pulse whose parameters are represented in Fig. 2(d) was tried ten times, always giving the same type of effect. The multidomain magnetic state observed in the track after a long and/or intense current pulse [Fig. 2(b)] typically corresponds to a demagnetized state, as can be obtained by heating the system above its Curie temperature, and then cooling it back in zero field.<sup>20</sup> The frontier line [Fig. 2(d)] between the  $(U, \Delta t)$  ranges corresponding to pulses with no effect [Fig. 2(a)], and to pulses leading to track demagneti-

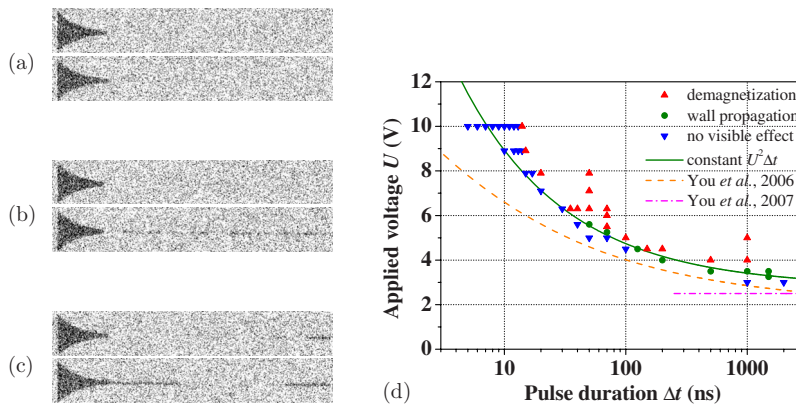


FIG. 2. (Color online) Effect of electrical current pulses, at zero applied field and at room temperature, on the remanent magnetic field induced domain structure of a 750 nm wide, He<sup>+</sup>-irradiated Pt/Co(0.5 nm)/Pt nanotrack with an out-of-plane magnetic anisotropy. (a)–(c) Typical magneto-optical difference images of the track before (top) and after (bottom): (a) a weak and/or short pulse, which produces no effect [downward triangles in (d)]; (b) a strong and/or long pulse, which provokes the demagnetization of the track [upward triangles in (d)]; (c) a pulse with intermediate strength and duration, which results in the propagation of existing domain walls [dots in (d)]. (d) Type of the observed effect, depending on the pulse voltage amplitude,  $U$ , and duration,  $\Delta t$  (here in log scale). The continuous line corresponds to a fit of the frontier line between the “demagnetizing” and “inefficient” pulse ranges to a law with constant Joule-deposited energy. The dashed and dash-dotted lines, respectively, correspond to estimates of the  $T = T_C = 365$  K isotherm curve, calculated as explained in the text (Refs. 30 and 31).

zation [Fig. 2(b)], respectively, is very well defined on 3 orders of magnitude of pulse duration. It should be emphasized that the observed effects only depend on the current-pulse duration and intensity and not at all on the pulse polarity. In particular, when propagation of the existing domain walls is observed [Fig. 2(c)], the direction of domain-wall propagation is independent of the direction of movement of the electrons which are supposed to induce spin transfer [see, for example, Fig. 2(c), where two domain walls propagate in opposite directions under the effect of the very same current pulse]. This implies that the observed current-induced domain-wall propagation is not due to spin transfer. Nor is it due to possible Oersted field effects since they should also depend on the current polarity.<sup>41</sup> The polarity-independent domain-wall propagation observed in Fig. 2(c) can rather be interpreted as resulting from Joule heating: if, during the pulse, the system is brought very close to its Curie temperature, domain-wall propagation becomes thermally activated.<sup>42</sup> The propagation direction is then determined by the small residual magnetic field (less than the 1 Oe dc propagation field at room temperature) that can always exist in our setup, and which favors the growth of one or the other domain type. This process is similar to the one involved in laser-assisted thermomagnetic recording.<sup>43</sup> It was verified experimentally, by artificially applying a small dc field, either upward or downward, during the current pulse, which allowed us to control the direction of domain-wall propagation. More data on this topic will be published elsewhere.<sup>35</sup>

### III. DISCUSSION

#### A. Joule heating of the track

When a current pulse flows into the nanotrack, Joule effect results into a heat generation, which, in a first approximation, is proportional to  $U^2\Delta t$ . When writing this, we neglect the effect of the track resistance increase during the pulse, which will be shown to be small in the following. Once heat has diffused in the track, it is finally dissipated in its environment, partly by metallic contacts at both of its ends<sup>44</sup> but mainly by the SiO<sub>2</sub>-covered substrate, which has a much larger contact surface with the track.<sup>30,31</sup> Current-pulse-induced temperature increases of up to several hundreds of kelvins, due to Joule heating, have been evidenced in very similar experiments on permalloy tracks,<sup>29,32,33</sup> and have been shown to occur starting from the nanosecond time scale.<sup>33</sup> According to these results, and given the typical spin-lattice relaxation time scale,<sup>45,46</sup> we can reasonably assert that heating of the spin system—and thus also thermomagnetic effects—can occur within the duration of the shortest pulses described in Fig. 2.

The observed frontier line, separating pulses with no effect from pulses leading to the track demagnetization, can be well fitted to a hyperbolic law, corresponding to a constant  $U^2\Delta t$  product, that is, to a constant heat dissipation in the nanotrack [Fig. 2(d)]. Therefore, it may correspond to the  $\Delta T = T_C - T_{\text{amb}}$  isotherm curve, where  $\Delta T$  is the temperature rise between the beginning and the end of the current pulse. This temperature rise was previously analytically calculated, taking into account heat dissipation in an insulating<sup>30</sup> or par-

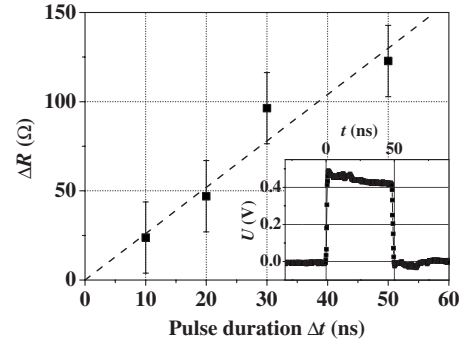


FIG. 3. Increase in a nanotrack's resistance,  $\Delta R$ , between the beginning and the end of a current pulse corresponding to  $U \approx 9$  V, as a function of the pulse duration,  $\Delta t$ . The dotted line is a linear fit to the  $\Delta R$  data, with a  $2.6 \text{ } \Omega \text{ ns}^{-1}$  slope. Inset: A typical oscillogram revealing the resistance increase and similar to those from which  $\Delta R$  values were extracted. The plotted voltage was measured across a  $50 \text{ } \Omega$  resistance, connected in series with the  $R \approx 0.9 \text{ k}\Omega$  nanotrack, during a  $50 \text{ ns}$  current pulse.

tially insulating substrate.<sup>31</sup> Following these results, we derived in both cases the resulting equation of the  $\Delta T = T_C - T_{\text{amb}}$  isotherm curve. The parameters used for the calculations are those given in Refs. 30 and 31, apart from the track length ( $L = 100 \text{ } \mu\text{m}$  for its narrowest segment) and resistance (again assumed as constant), and the SiO<sub>2</sub> coverage thickness on the substrate. Even if they do not perfectly fit to the experimentally observed frontier line, the resulting curves [Fig. 2(d)] reproduce the order of magnitude of the pulse amplitudes and durations corresponding to the crossover between inefficient and demagnetizing pulses. The observed misfit may be explained by heat dissipation through the contacts at both ends of the wire, which is not taken into account here.<sup>30,31,44</sup> Moreover, the hypothesis of a stationary and uniform thermal regime in the track gets less and less valid when the pulse duration is reduced, which can explain the enhanced misfit in the shortest pulse range.<sup>30,31</sup>

To further validate our interpretation of Fig. 2(d), we monitored in real time the resistance of a similar nanotrack during current pulses,<sup>29,32,33</sup> by measuring the voltage across a  $50 \text{ } \Omega$  resistance connected in series with the nanotrack. A typical oscillogram, for a pulse corresponding to  $U \approx 9$  V, is shown in the inset of Fig. 3: the measured voltage clearly decreases during the pulse, which is related to a resistance increase,  $\Delta R$ , of the nanotrack, due to Joule heating.  $\Delta R$ , measured at the end of the current pulse, is plotted in Fig. 3 as a function of the pulse duration, and can be fitted to a linear increase by  $2.6 \text{ } \Omega \text{ ns}^{-1}$ . The temperature increase in the nanotrack is directly connected to the  $\Delta R$  value, via a temperature coefficient,  $\chi = [1/R(T_{\text{amb}})](\Delta R/\Delta T)$ . Starting from standard, bulk values of  $\chi$  (in the 273–373 K temperature range,<sup>47</sup>  $\chi_{\text{Pt}} = 3.92 \times 10^{-3} \text{ K}^{-1}$ , and  $\chi_{\text{Co}} = 6.04 \times 10^{-3} \text{ K}^{-1}$ ), and taking into account their reduction in metallic films whose thickness is comparable to or smaller than the electron mean free path (around 10 nm for the metals used here),<sup>48</sup> a global  $\chi$  coefficient can be estimated for the whole nanotrack,  $\chi \approx 2 \times 10^{-3} \text{ K}^{-1}$ . This allows us to estimate that the nanotrack heats by  $1.4 \text{ K ns}^{-1}$  for a  $U \approx 9$  V pulse. This means that for such current pulses, starting from

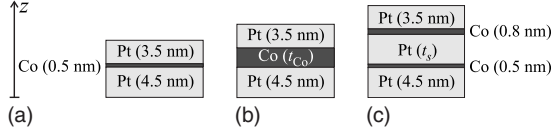


FIG. 4. Structures of the investigated samples: (a) the Pt/Co(0.5 nm)/Pt stack described in Sec. II; (b) the Pt/Co( $t_{\text{Co}}$ )/Pt stacks addressed in Fig. 5; (c) the spin valves measured in Fig. 6. The definition of the  $z$  coordinate used in the text is indicated.

$T_{\text{amb}}=300$  K, the Curie temperature,  $T_C=365$  K, is reached within 46 ns, which is quite compatible with Fig. 2(d). For such a temperature rise, the track resistance increases by about 13% of its initial value, which is relatively low, and does not strongly contradict the validity of the initial assumption of a  $U^2\Delta t$  heat generation.

## B. Spin-polarized current in the cobalt layer

### 1. Fuchs-Sondheimer model

To explain the absence of spin transfer effect, in particular for current pulses with intensities and durations lower than those of pulses which result in the track demagnetization, we now focus on the evaluation of the spin-polarized current density in the cobalt layer of our metallic stack [Fig. 4(a)], which is indeed the relevant quantity for estimating the spin transfer efficiency. The simplest approach to describe electron transport in metallic layers whose thickness is comparable to or smaller than the electron mean free path is based on the semiclassical Fuchs-Sondheimer model.<sup>49-51</sup> It takes into account the enhanced interface contributions to electron scattering in such layers,<sup>49,50</sup> as compared to bulk resistivity, usually described in the frame of the Drude-Sommerfeld model. When including spin-dependent electron scattering,<sup>52,53</sup> it has also been shown to provide a simple and physical understanding of giant magnetoresistance in magnetic multilayers.

In its full generality, this model requires a very large number of parameters, necessary to describe each material and interface, at the expense of a good legibility. To describe our system, we chose to make several assumptions, in order to keep only the most meaningful of these parameters. Namely, each material is described by an electron mean free path,  $\ell$ , and a resistivity,  $\rho$ , that both depend on the electron spin (majority,  $\uparrow$ , or minority,  $\downarrow$ ) for cobalt.<sup>54</sup> Using the usual bulk spin asymmetry parameter,  $\alpha=\rho_{\downarrow}/\rho_{\uparrow}$ , the values of  $\rho$  and  $\ell$  for each spin channel can be expressed in terms of the overall cobalt resistivity,  $\rho_{\text{Co}}$ , and mean free path,  $\ell_{\text{Co}}$ ,

$$\rho_{\text{Co}\uparrow} = \rho_{\text{Co}} \frac{1 + \alpha}{\alpha}, \quad \ell_{\text{Co}\uparrow} = \ell_{\text{Co}} \frac{2\alpha}{1 + \alpha}, \quad (1a)$$

$$\rho_{\text{Co}\downarrow} = \rho_{\text{Co}}(1 + \alpha), \quad \ell_{\text{Co}\downarrow} = \ell_{\text{Co}} \frac{2}{1 + \alpha}. \quad (1b)$$

The density of conduction electrons (thought of as a single band of free electrons) and the effective electron mass are assumed to be the same in platinum and cobalt, and to be independent of spin, which implies that the electrical con-

ductivity,  $\sigma=1/\rho$ , is equivalent (proportional with a fixed coefficient) to an electron collision time,  $\tau$ . This collision time disappears in the  $\rho\ell$  product (such as in the Drude formula), which is a material-specific constant, independent of spin, and proportional with a fixed coefficient to the Fermi velocity,  $v_F$ . At interfaces between cobalt and platinum, an electron is assumed to be either transmitted without any change in its velocity direction (probability  $T$ ), or randomly scattered, with a loss of all memory on its previous velocity. As interface transmission obviously depends on spin, separate coefficients,  $T_{\uparrow}$  and  $T_{\downarrow}$ , are introduced to describe the two spin channels. Their difference is described by a spin asymmetry coefficient,  $N$ , defined as

$$N = \frac{1 - T_{\downarrow}}{1 - T_{\uparrow}}. \quad (2)$$

Specular reflection at interfaces is not considered here. At the outer surfaces of the stack, the original Fuchs-Sondheimer specular reflection parameter,  $p$ , is used<sup>49-51</sup> while a diffuse reflection of the electron takes place with a probability  $1-p$ . The surface and interface parameters,  $p$  and  $T$ , are assumed not to depend on the incidence angle, unlike in the quantumlike models.<sup>55</sup>

In our case, [Fig. 4(a)], the thickness of the whole Pt/Co/Pt stack is of the order of magnitude of the electron mean free path, which is known to be lower than (or, at most, equal to) the spin-diffusion length,  $\ell_{\text{sf}}$ .<sup>56</sup> The relevance of spin-flip effects in our system in thus, *a priori*, unclear. Therefore, a first series of calculations was performed without considering any spin-flip processes across the stack: the Boltzmann equation was solved separately for the two spin channels, considered as independent.<sup>57</sup> As specular reflection at interfaces is not introduced in this model, its solution can be explicitly written down for any number of layers,  $n$ . Only a one-dimensional numerical integration, over the incidence angle of the electron on interfaces, is required to evaluate the spin-polarized current density at a given height,  $z$ , across the stack. In a second series of calculations, spin-flip scattering was introduced, either in the bulk of platinum layers, through a spin-flip collision time,  $\tau_{\uparrow\downarrow}$ , or at the Co/Pt interfaces, by a spin-flip transmission coefficient,  $T_{\uparrow\downarrow}$ . In the first case, a different rotation in spin space has to be performed in each layer, in order to obtain the eigenmodes of the Boltzmann equation (depending on  $\tau_{\uparrow\downarrow}$ , these modes can correspond either to  $[\uparrow, \downarrow]$ - or to  $[\text{charge}, \text{spin}]$ -type vectors). As a consequence, an explicit solution no longer exists; for each value of the electron incidence angle, a  $4n \times 4n$  matrix has to be inverted. Note that, with such a formalism, specular reflection at interfaces can be included with no additional calculation cost. Spin flip in the bulk of the 0.5-nm-thick cobalt layer is considered as negligible and, thus, is not taken into account.

### 2. Parameters for describing Co/Pt stacks

The numerical values of the resistivities, mean free paths, and an estimate for the surface specular reflection parameter,  $p$ , of platinum were altogether determined by measuring (at room temperature with a four-probe technique) the apparent

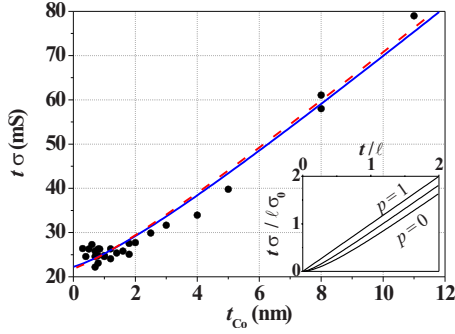


FIG. 5. (Color online) Measured sheet conductance, at room temperature, of Pt(4.5 nm)/Co( $t_{\text{Co}}$ )/Pt(3.5 nm) trilayers with different cobalt thicknesses,  $t_{\text{Co}}$  (dots). Each data point corresponds to one sample. The curves were obtained by numerical calculations within the Fuchs-Sondheimer model, with  $T_{\perp}=0.1$ , either without spin flip (full curve, with  $T_{\perp}=0.22$ , i.e.,  $N=1.15$  and  $p=0.42$ ), or with bulk spin flip in platinum (dashed curve, with  $T_{\perp}=0.33$ , i.e.,  $N=1.35$  and  $p=0.33$ ). The values of the other parameters are those given in the text.  $t$  stands for the total thickness of the stack. The inset recalls the Fuchs-Sondheimer result for a single thin film, for  $p=0, 0.5$ , and  $1$  ( $\sigma_0$  is the bulk conductivity).

in-plane sheet conductances of Pt and Co single layers. These data were analyzed with the Fuchs-Sondheimer model, leading to a set of parameters that allow experimental data to be reproduced. In particular, the inset of Fig. 5 recalls the result of a Fuchs-Sondheimer calculation for a single thin film,<sup>49,50</sup> and shows that the value of the  $p$  parameter directly controls the thickness dependence of the calculated sheet conductance. From thick platinum single films, with different thicknesses, we estimated  $\rho_{\text{Pt}}=17.45 \mu\Omega \text{ cm}$ , and deduced  $\ell_{\text{Pt}}=13.11 \text{ nm}$ , from a mean of published values of the  $\rho_{\text{Pt}}\ell_{\text{Pt}}$  product.<sup>50,58</sup> From the thickness dependence of the sheet conductance, the  $p$  parameter was found to be about 0.6, and was left as an adjustable parameter for the stacks described in the following. For cobalt, the overall resistivity and mean free path were found to be  $\rho_{\text{Co}}=17.7 \mu\Omega \text{ cm}$  and  $\ell_{\text{Co}}=5.2 \text{ nm}$ , consistently with literature.<sup>50,58</sup> Given the low cobalt thickness with respect to the electron mean free path in the sample described in Sec. II, the role of bulk spin scattering in cobalt is expected to be negligible, and the value of  $\alpha$  is thus anticipated to be of minor importance. It was set to  $\alpha=3$ .<sup>53,59</sup> Note that the values of platinum and cobalt resistivities are close to each other. This means that, taking into account only the bulk resistivities, one would expect the charge current in cobalt to reach about 5.8% of the total charge current in the Pt/Co/Pt stack (0.5 nm of cobalt within a total thickness of 8.5 nm).

The interface transmission coefficients,  $T_{\uparrow}$  and  $T_{\downarrow}$ , are the most important parameters within this simple model, as far as spin polarization is concerned. They were similarly estimated from the sheet conductances of Pt(4.5 nm)/Co( $t_{\text{Co}}$ )/Pt(3.5 nm) trilayers [Fig. 4(b)], where only the cobalt layer thickness,  $t_{\text{Co}}$ , was changed. Figure 5 shows the evolution of the sheet conductance,  $t\sigma$  (here,  $t$  is the total thickness of the stack), as a function of  $t_{\text{Co}}$ . For thick cobalt layers (as compared to  $\ell_{\text{Co}}$ ), the sheet conductances of the three layers of the stack simply add, and a

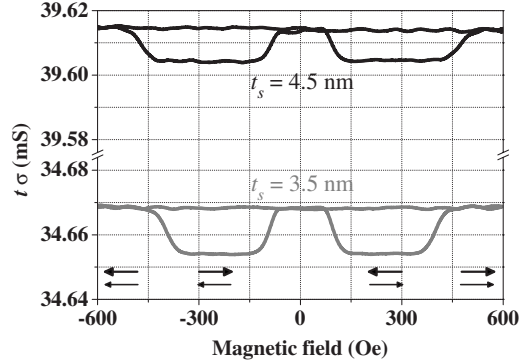


FIG. 6. Measured sheet conductance as a function of magnetic field for two Pt(4.5 nm)/Co(0.5 nm)/Pt( $t_s$ )/Co(0.8 nm)/Pt(3.5 nm) spin-valve bilayers (Ref. 60). These magnetoconductance loops show well-defined plateaus corresponding to parallel (P) and antiparallel (AP) spin-valve configurations.  $t$  stands for the total thickness of the stack.

linear behavior of  $t\sigma$  with respect to  $t_{\text{Co}}$  is expected. Besides, the positive curvature of the low cobalt thickness data can be understood from the inset of Fig. 5. On this graph, a curvature is shown to appear on a single film sheet conductance curve when the surface specularity parameter,  $p$ , is reduced, that is when nonzero interface scattering occurs.<sup>49,50</sup> In the case of a cobalt layer embedded in a Pt/Co/Pt trilayer, the  $p$  parameter, designed to describe single layers, is not relevant. It is replaced by the interface transmission coefficient,  $T$ . The observed curvature, typical of a nonzero interface scattering, means that a low  $T$  factor at the Co/Pt interfaces is required. This implies a reduction in the charge current in the cobalt layer, as compared to that expected when taking into account only bulk resistivities.

To know more about the spin-dependent transmission coefficients,  $T_{\uparrow}$  and  $T_{\downarrow}$ , and hence about the spin-polarized current in the cobalt layer, sheet conductances in the parallel (P) and antiparallel (AP) states of several Pt(4.5 nm)/Co(0.5 nm)/Pt( $t_s$ )/Co(0.8 nm)/Pt(3.5 nm) spin valves [Fig. 4(c)], with an out-of-plane anisotropy,<sup>60</sup> were measured. As shown in Fig. 6, the sheet conductance levels in the P and AP states have a small<sup>61,62</sup> but measurable difference (11  $\mu\text{S}$  for  $t_s=4.5 \text{ nm}$ ). Moreover, the sheet magnetoconductance decreases when the platinum spacer thickness increases. The data displayed in the lower panel of Fig. 7 result from our calculation within the Fuchs-Sondheimer model, in the three cases considered in the following, using the aforementioned set of parameters, and adjusting the value of the surface specularity parameter,  $p$ , so as to reproduce the data shown in Fig. 5. As is already well known for in-plane magnetized spin valves with thicknesses of a few nanometers,<sup>52,63</sup> these data show that the sheet magnetoconductance of a Pt/Co/Pt/Co/Pt spin valve is controlled by the interface spin-scattering asymmetry,  $N$ . Therefore, a specific value of  $N$  ( $\neq 1$ ) is required in order to reproduce the experimental value of the magnetoconductance (dash-dotted line in Fig. 7). This  $N$  value can *a priori* correspond to several ( $T_{\uparrow}, T_{\downarrow}$ ) couples. As discussed above, interface transmission is expected to be low. Therefore, we chose to assume  $T_{\downarrow}=0.1$  for these calculations, and then deduced from Fig. 7 the

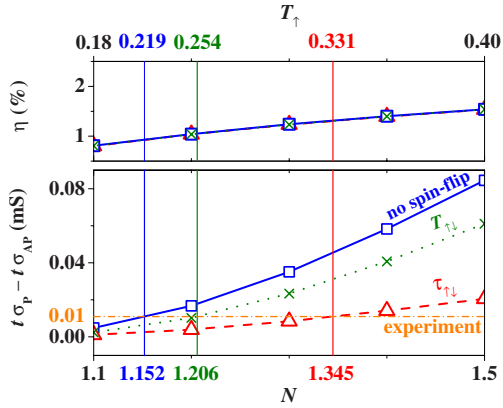


FIG. 7. (Color online) Calculated variation in the sheet magnetoconductance, for the spin valve with  $t_s=4.5$  nm, as a function of the interface spin-scattering asymmetry parameter,  $N$  (lower panel). The minority interface transmission is fixed at  $T_\downarrow=0.1$ . The upper panel shows the corresponding calculated ratio,  $\eta$ , between the spin-polarized current in the cobalt layer and the total charge current in the Pt/Co(0.5 nm)/Pt stack, as well as  $T_\uparrow$  values corresponding to the  $N$  scale. For both panels, squares correspond to values obtained without spin flip. Triangles and crosses correspond to those obtained while, respectively, taking into account bulk spin-flip scattering in platinum, and Co/Pt interface spin-flip scattering. The dash-dotted line indicates the measured value of the sheet magnetoconductance, namely, 11  $\mu$ S.  $t$  stands for the total thickness of the stack.

corresponding values of  $N$  and  $T_\uparrow$ , in order to match the measured magnetoconductance.

### 3. Spin-polarized current density without spin flip

Disregarding any spin-flip effects to begin with,  $T_\uparrow=0.22$  together with  $T_\downarrow=0.1$  (that is,  $N=1.15$ ) allow us to match the measured magnetoconductance value (Fig. 7, lower panel). Besides, by numerical calculation within the Fuchs-Sondheimer model, with the same parameters, the full curve in Fig. 5 is obtained. It also appears to satisfactorily reproduce our Pt/Co/Pt sheet conductance experimental data, provided an adjustment of the specularity parameter,  $p$ , at the outer surfaces of the stack (changing its value only shifts the

whole curve vertically, without affecting its slope and curvature). Applying now the same set of parameters to the Pt/Co(0.5 nm)/Pt sample, which shows no detectable spin transfer torque effect on domain walls (Sec. II), we evaluate the charge current in the cobalt layer to be 3.36% of the total current in the sample, and the spin-polarized current only 0.93% (Fig. 7, upper panel), which corresponds to a polarization  $P=0.28$  in the cobalt layer. The corresponding local conductivity profiles in the two conduction channels, as a function of the  $z$  position across the stack [Fig. 4(a)], are plotted in Fig. 8(a). As a consequence of the low interface transmission, the current density is strongly reduced in the cobalt layer as compared to that expected from its bulk resistivity. Spin polarization of the current is largest in the cobalt, but, as one can see Fig. 8(a), it also extends in the platinum layers, where the spin-polarized currents are, respectively, 0.97% and 0.91% of the total current.

### 4. Effect of bulk spin-flip scattering in platinum

For calculations taking into account spin flip in bulk platinum, consistently with experimental evidence of the spin-diffusion length being on the order of the electron mean free path,<sup>56</sup> and taking care of keeping unchanged the overall resistivity, the spin-flip collision time,  $\tau_{\uparrow\downarrow}$ , and the spin-conserving collision times,  $\tau_{\uparrow\uparrow}$  and  $\tau_{\downarrow\downarrow}$ , were all set equal to  $2\tau_{Pt}$ . As one can see Fig. 7, introducing such spin-flip scattering in the platinum layers, while keeping all other parameters unchanged, does not have a direct influence on spin-polarized current in the cobalt layer of the Pt/Co(0.5 nm)/Pt stack. This results from the weakness of interface transmissions that nearly insulates the cobalt layer from the platinum ones. On the other hand, the sheet magnetoconductance in Pt/Co/Pt/Co/Pt, that results from a crosstalk between both cobalt layers in the spin valve, through the platinum spacer, is markedly reduced, as compared to the case without spin flip (Fig. 7). This is remarkable since the platinum spacer thickness is only one half of the characteristic spin-flip length,  $v_F\tau_{\uparrow\downarrow}$ . To compensate this effect, the interface spin-scattering asymmetry,  $N$ , has to be assumed as larger, namely,  $N\approx 1.35$ , in order to match the experimental value of the sheet magnetoconductance. Still keeping  $T_\downarrow=0.1$ , this implies that transmission of majority electrons at interfaces

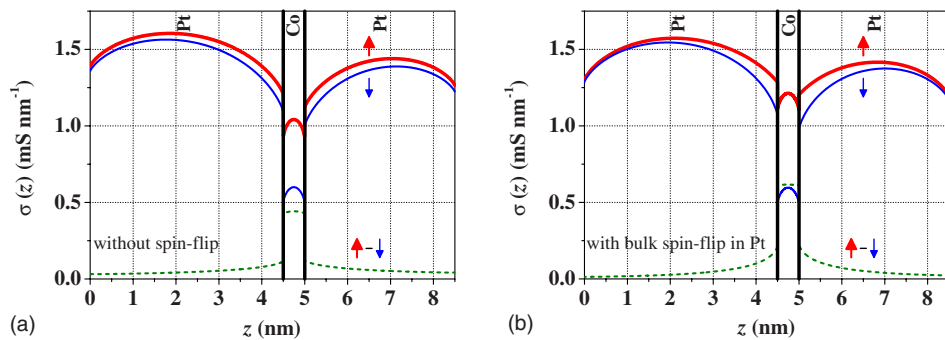


FIG. 8. (Color online) Calculated profiles of the spin-resolved conductivities for a Pt(4.5 nm)/Co(0.5 nm)/Pt(3.5 nm) stack, in cases without spin flip (a) and with bulk spin flip in platinum (b). The spin-polarized conductivity is also shown. Parameters of the calculation are the same as in Fig. 5. The integrated sheet conductance of the whole stack is 23.6 mS in case (a) and 23.4 mS in case (b). For comparison, the values of the bulk conductivity are 5.73 and 5.65  $\text{mS nm}^{-1}$  for platinum and cobalt, respectively.

is increased to  $T_{\uparrow}=0.33$ . Figure 5 (dashed curve) shows that, in this case, providing a small change in the surface specular parameter,  $p$ , the experimental sheet conductance data are also well reproduced. This indirectly results in an increase in the spin-polarized current in the cobalt layer of the Pt/Co/Pt stack, when taking into account spin-flip scattering (Fig. 7). This result, counterintuitive at first sight, is linked to the way we determine the model parameters from the experimental data. Namely, with spin flip and the corresponding set of parameters, we obtain a slightly higher charge current in the cobalt layer (3.75% of the total current), as well as a larger spin-polarized current (1.32% of the total current, which corresponds to a polarization  $P=0.35$ ). The spin-polarized current in the platinum layers is still around 0.9%. The new profiles of the spin-resolved conductivities across the stack are plotted in Fig. 8(b). The faster decrease in spin polarization in platinum, when the distance from the cobalt layer increases, can be clearly seen, as well as the higher majority-spin current in the cobalt layer, due to the higher value of  $T_{\uparrow}$ .

### 5. Effect of interface spin-flip scattering

To evaluate the influence of spin flip at the Co/Pt interface transmission, a 0.5 spin-flip probability was introduced while still keeping unchanged the total transmission of minority electrons,  $T_{\downarrow}=0.1$ . This way, a minority electron has a probability  $T_{\downarrow\downarrow}=0.05$  to be transmitted with conserving its spin, and a probability  $T_{\downarrow\uparrow}=0.05$  to experience a spin-flip transmission. Majority electrons are treated in the same way, though with an adjusted value of their total transmission,  $T_{\uparrow}$ , which is driven by the interface spin-scattering asymmetry,  $N$ . As shown in Fig. 7, the effect of interface spin flip is very similar to that of the bulk spin flip: the sheet magnetoconductance is (less) reduced and the spin-polarized current in the cobalt layer is unchanged. Here again, in order to reach the experimental level of sheet magnetoconductance,  $N$  has to be increased to 1.21, leading to a proportion 1.03% of spin-polarized current in the cobalt layer. This value falls in between the two values previously obtained. However, the relevance of this type of spin flip is not obvious: the dependence of the sheet magnetoconductance on the platinum spacer thickness corresponds more to bulk spin-flip scattering in platinum, that is, moreover, known to be strong.<sup>56</sup>

### 6. Spin-transfer versus Joule-heating balance

Summarizing, the calculations detailed above show that: (i) current—and all the more spin-polarized current—in the cobalt layer corresponds to a very low proportion of the total current flowing in the Pt/Co/Pt stack; (ii) the ratio between spin-polarized current in cobalt and total current in the stack is weakly affected by the presence of spin-flip scattering, either in the bulk of platinum, or at Co/Pt interfaces. This last point is due to a very weak interface transmission of electrons at Co/Pt interfaces, which results in nearly insulating the cobalt layer from the rest of the stack. The thin gold layer that remains from the etching mask on top of the tracks was not explicitly taken into account here. However, its inclusion in our model would only result in considering a  $T$ -type inter-

face instead of the upper,  $p$ -type surface of Pt/Co/Pt, which, as discussed above, weakly impacts spin-polarized transport in cobalt.

To discuss the consequences of these results on spin transfer torque efficiency in a Pt/Co/Pt nanotrack, we now have to come back to spin-polarized current *densities*. From this point of view, among the three cases treated above, the most optimistic one is the second one, where spin flip in bulk platinum is taken into account. Even in this case, the spin-polarized current density expected in the cobalt layer of the track is only  $6.15 \times 10^9 \text{ A m}^{-2}$  per applied volt, that is, about two orders of magnitude lower than what was expected from an oversimplified uniform-current-density assumption. This means that, for the maximum voltage of 10 V that we could apply to our nanotrack because of Joule heating [Fig. 2(d)], the maximum spin-polarized current density in cobalt remained below  $10^{11} \text{ A m}^{-2}$ . This is more than one order of magnitude lower than the  $10^{12} \text{ A m}^{-2}$  current-density range where spin-transfer-induced domain-wall motion is usually observed in similar systems,<sup>20-25</sup> which seems to explain that we could not evidence any spin transfer effects. This result is due to an unfavorable balance between spin transfer torque and Joule heating in our system, where only 1% of the electrons which provoke Joule heating can actually exert a torque on a domain wall: the (low) Curie temperature is reached for spin-polarized current densities still insufficient to make a domain wall propagate in the track.

## IV. CONCLUSIONS AND PERSPECTIVES

The effects of an electrical current on the magnetic domain structure in a He<sup>+</sup>-irradiated Pt/Co(0.5 nm)/Pt nanotrack with out-of-plane anisotropy were studied through current-injection experiments and electron-transport calculations. We showed that, in this system, current pulses with durations varying on 3 orders of magnitude, and with intensities limited by Joule heating of the track above its low Curie temperature, only had thermal effects, and, in particular, did not cause any detectable spin transfer. Thanks to calculations within a Fuchs-Sondheimer model adapted to our system, this was ascribed to the low proportion of spin-polarized current flowing in the track's ultrathin cobalt layer, as compared to the total current in the track, which is mainly due to the low transmission of electrons at Co/Pt interfaces.

This leads us to emphasize that, among other parameters, the relative efficiencies of Joule heating and spin-polarized electron transport should be carefully considered when attempting to select a system for spin transfer torque driven domain-wall propagation: on top of spin transfer torque intensity, and of domain-wall depinning and propagation thresholds, the fact that a sufficient spin-polarized current density can be injected in the system without provoking an excessive Joule heating is also crucial. This last point mainly depends on the spin-polarized electron-transport properties, Curie temperature, and thermal dissipation in the sample. It is, however, worth to note that bringing a magnetic system very close to its Curie temperature for a short period of time can allow extremely fast magnetization reversal processes, as was recently shown, for instance, in the case of ultrafast laser-induced magnetization reversal.<sup>64</sup>

Our Fuchs-Sondheimer approach is quite general, and can be applied to other metallic systems, with either in-plane<sup>7-9</sup> or out-of-plane magnetic anisotropy.<sup>20-25</sup> In particular, it could help to understand three systems very similar to ours, namely, Co/Pt multilayers,<sup>21</sup> Co/Ni multilayers,<sup>24,25</sup> and Pt/Co/AlOx,<sup>20</sup> where spin transfer induced domain-wall depinning and/or propagation were recently evidenced. These three systems all have a higher amount of magnetic matter with respect to the total amount of conductive matter, which may increase the ratio between the spin-polarized current density in the magnetic layers and the total current density in the tracks. Pt/Co/AlOx, whose structure differs from ours only by replacing one of the platinum layers by an insulating layer, is of particular interest. Apart from the obvious improvement in the spin-transfer versus Joule-heating balance, due to the reduction in the total platinum thickness, and to a somewhat higher Curie temperature,<sup>20</sup> the nature of one of the cobalt layer's interfaces is changed in this system, from the metal/metal type (described above by a  $T$  transmission parameter) to the metal/insulator type (described by a  $p$

specular reflection parameter). Consequences of such a difference need to be addressed in more detail.

It should be finally stressed that the Fuchs-Sondheimer model, based on a continuous Boltzmann equation, is here at the limit of its validity, as it is applied to ultrathin films of a few atomic layers. A quantumlike treatment of electron conduction in such ultrathin films is therefore desirable.

#### ACKNOWLEDGMENTS

S. Rohart and J.-P. Adam are gratefully acknowledged for assistance with the measurements, as well as M. Bottineau for technical support. This research was performed in the frame of a collaboration between Univ. Paris-Sud and ALTIS Semiconductor. M.C. thanks the latter and the French ANRT for CIFRE financial support. This work was also partially supported by the EU-“Research Infrastructures Transnational Access” program “Center for Application of Ion Beams in Materials Research” under Contract No. 025646, and by the French ANR-07-NANO-034 “Dynawall” project.

\*Present address: Institute for Molecules and Materials, Radboud University Nijmegen, 6525 AJ Nijmegen, The Netherlands; m.cormier@science.ru.nl

<sup>1</sup>L. Thomas and S. Parkin, in *Handbook of Magnetism and Advanced Magnetic Materials*, edited by H. Kronmüller and S. Parkin (Wiley, Chichester, 2007), Vol. 2, pp. 942–982.

<sup>2</sup>D. A. Allwood, G. Xiong, C. C. Faulkner, D. Atkinson, D. Petit, and R. P. Cowburn, *Science* **309**, 1688 (2005).

<sup>3</sup>S. S. P. Parkin, M. Hayashi, and L. Thomas, *Science* **320**, 190 (2008).

<sup>4</sup>L. Berger, *J. Appl. Phys.* **49**, 2156 (1978).

<sup>5</sup>L. Berger, *J. Appl. Phys.* **55**, 1954 (1984).

<sup>6</sup>L. Berger, *Phys. Rev. B* **33**, 1572 (1986).

<sup>7</sup>A. Yamaguchi, T. Ono, S. Nasu, K. Miyake, K. Mibu, and T. Shinjo, *Phys. Rev. Lett.* **92**, 077205 (2004).

<sup>8</sup>N. Vernier, D. A. Allwood, D. Atkinson, M. D. Cooke, and R. P. Cowburn, *Europhys. Lett.* **65**, 526 (2004).

<sup>9</sup>M. Kläui, C. A. F. Vaz, J. A. C. Bland, W. Wernsdorfer, G. Faini, E. Cambril, L. J. Heyderman, F. Nolting, and U. Rüdiger, *Phys. Rev. Lett.* **94**, 106601 (2005).

<sup>10</sup>*Current Perspectives on Spin Transfer Torque*, *J. Magn. Magn. Mater.* **320**, 1190–1311 (2008).

<sup>11</sup>C. H. Marrows, *Adv. Phys.* **54**, 585 (2005).

<sup>12</sup>G. Tatara, H. Kohno, and J. Shibata, *J. Phys. Soc. Jpn.* **77**, 031003 (2008).

<sup>13</sup>S.-W. Jung, W. Kim, T.-D. Lee, K.-J. Lee, and H.-W. Lee, *Appl. Phys. Lett.* **92**, 202508 (2008).

<sup>14</sup>S. Fukami, T. Suzuki, N. Ohshima, K. Nagahara, and N. Ishiwata, *J. Appl. Phys.* **103**, 07E718 (2008).

<sup>15</sup>D. Ravelosona, F. Cayssol, J. Wunderlich, H. W. Schumacher, C. Chappert, V. Mathet, J. Ferré, and J.-P. Jamet, *J. Magn. Magn. Mater.* **249**, 170 (2002).

<sup>16</sup>P. J. Metaxas, J. P. Jamet, A. Mougin, M. Cormier, J. Ferré, V. Baltz, B. Rodmacq, B. Dieny, and R. L. Stamps, *Phys. Rev. Lett.* **99**, 217208 (2007).

<sup>17</sup>G. Tatara and H. Kohno, *Phys. Rev. Lett.* **92**, 086601 (2004).

<sup>18</sup>A. Thiaville, Y. Nakatani, J. Miltat, and Y. Suzuki, *Europhys. Lett.* **69**, 990 (2005).

<sup>19</sup>A. Mougin, M. Cormier, J. P. Adam, P. J. Metaxas, and J. Ferré, *EPL* **78**, 57007 (2007).

<sup>20</sup>T. A. Moore, I. M. Miron, G. Gaudin, G. Serret, S. Auffret, B. Rodmacq, A. Schuhl, S. Pizzini, J. Vogel, and M. Bonfim, *Appl. Phys. Lett.* **93**, 262504 (2008).

<sup>21</sup>O. Boulle, J. Kimling, P. Warnicke, M. Kläui, U. Rüdiger, G. Malinowski, H. J. M. Swagten, B. Koopmans, C. Ulysse, and G. Faini, *Phys. Rev. Lett.* **101**, 216601 (2008).

<sup>22</sup>H. Tanigawa, K. Kondou, T. Koyama, K. Nakano, S. Kasai, N. Ohshima, S. Fukami, N. Ishiwata, and T. Ono, *Appl. Phys. Express* **1**, 011301 (2008).

<sup>23</sup>T. Koyama, G. Yamada, H. Tanigawa, S. Kasai, N. Ohshima, S. Fukami, N. Ishiwata, Y. Nakatani, and T. Ono, *Appl. Phys. Express* **1**, 101303 (2008).

<sup>24</sup>H. Tanigawa, T. Koyama, G. Yamada, D. Chiba, S. Kasai, S. Fukami, T. Suzuki, N. Ohshima, N. Ishiwata, Y. Nakatani, and T. Ono, *Appl. Phys. Express* **2**, 053002 (2009).

<sup>25</sup>C. Burrowes, A. P. Mihai, D. Ravelosona, J.-V. Kim, C. Chappert, L. Vila, A. Marty, Y. Samson, F. Garcia-Sanchez, L. D. Buda-Prejbeanu, I. Tudosa, E. E. Fullerton, and J.-P. Attané, *Nat. Phys.* **6**, 17 (2010).

<sup>26</sup>G. Tatara, T. Takayama, H. Kohno, J. Shibata, Y. Nakatani, and H. Fukuyama, *J. Phys. Soc. Jpn.* **75**, 064708 (2006).

<sup>27</sup>M. E. Lucassen, H. J. van Driel, C. Morais Smith, and R. A. Duine, *Phys. Rev. B* **79**, 224411 (2009).

<sup>28</sup>C. Chappert, H. Bernas, J. Ferré, V. Kottler, J.-P. Jamet, Y. Chen, E. Cambril, T. Devolder, F. Rousseaux, V. Mathet, and H. Launois, *Science* **280**, 1919 (1998).

<sup>29</sup>A. Yamaguchi, S. Nasu, H. Tanigawa, T. Ono, K. Miyake, K. Mibu, and T. Shinjo, *Appl. Phys. Lett.* **86**, 012511 (2005).

<sup>30</sup>C.-Y. You, I. M. Sung, and B.-K. Joe, *Appl. Phys. Lett.* **89**, 222513 (2006).

- <sup>31</sup>C.-Y. You and S.-S. Ha, *Appl. Phys. Lett.* **91**, 022507 (2007).
- <sup>32</sup>M. Hayashi, L. Thomas, C. Rettner, X. Jiang, and S. S. P. Parkin, *EPL* **78**, 67006 (2007).
- <sup>33</sup>L. Thomas, M. Hayashi, X. Jiang, C. Rettner, and S. S. P. Parkin, *Appl. Phys. Lett.* **92**, 112504 (2008).
- <sup>34</sup>J. Ferré, C. Chappert, H. Bernas, J.-P. Jamet, P. Meyer, O. Kaitsov, S. Lemerle, V. Mathet, F. Rousseaux, and H. Launois, *J. Magn. Magn. Mater.* **198-199**, 191 (1999).
- <sup>35</sup>M. Cormier *et al.* (unpublished).
- <sup>36</sup>T. Devolder, J. Ferré, C. Chappert, H. Bernas, J.-P. Jamet, and V. Mathet, *Phys. Rev. B* **64**, 064415 (2001).
- <sup>37</sup>J. Ferré, V. Repain, J.-P. Jamet, A. Mougin, V. Mathet, C. Chappert, and H. Bernas, *Phys. Status Solidi A* **201**, 1386 (2004).
- <sup>38</sup>Picoprobe®, <http://www.ggb.com>
- <sup>39</sup>This resistance value is much lower than that expected from the track dimensions, given the bulk resistivities of cobalt and platinum. This is due to a thin gold layer remaining from the etching mask on top of the Pt/Co/Pt track, whose exact thickness is unknown, and which results in a reduction in the measured apparent resistance.
- <sup>40</sup>Our optical method is sensitive to a typical domain-wall displacement of about 1  $\mu\text{m}$ . To ensure that the effect of the shortest current pulses could be detected, these pulses were applied by series, within which the total duration of current application was maintained above 200 ns. This means that the smallest domain-wall propagation velocity that we could detect was around 5  $\text{m s}^{-1}$ .
- <sup>41</sup>O. Boulle, L. Heyne, J. Rhensius, M. Kläui, U. Rüdiger, L. Joly, L. Le Guyader, F. Nolting, L. J. Heyderman, G. Malinowski, H. J. M. Swagten, B. Koopmans, C. Ulysse, and G. Faini, *J. Appl. Phys.* **105**, 07C106 (2009).
- <sup>42</sup>J. Ferré, in *Spin Dynamics in Confined Magnetic Structures I*, Topics in Applied Physics Vol. 83, edited by B. Hillebrands and K. Ounadjela (Springer, Berlin, 2002), pp. 127–165.
- <sup>43</sup>M. Mansuripur, *The Physical Principles of Magneto-Optical Recording* (Cambridge University Press, Cambridge, 1995).
- <sup>44</sup>C. Durkan, M. A. Schneider, and M. E. Welland, *J. Appl. Phys.* **86**, 1280 (1999).
- <sup>45</sup>E. Beaurepaire, J.-C. Merle, A. Daunois, and J.-Y. Bigot, *Phys. Rev. Lett.* **76**, 4250 (1996).
- <sup>46</sup>G. Zhang, W. Hübner, E. Beaurepaire, and J.-Y. Bigot, in *Spin Dynamics in Confined Magnetic Structures I*, Topics in Applied Physics Vol. 83, edited by B. Hillebrands and K. Ounadjela (Springer, Berlin, 2002), pp. 245–290.
- <sup>47</sup>C. J. Smithells, *Metals Reference Book*, 4th ed. (Butterworths, London, 1967).
- <sup>48</sup>W. F. Leonard and R. L. Ramey, *J. Appl. Phys.* **37**, 3634 (1966).
- <sup>49</sup>E. H. Sondheimer, *Adv. Phys.* **1**, 1 (1952).
- <sup>50</sup>K. L. Chopra, *Thin Film Phenomena* (McGraw-Hill, New York, 1969), pp. 344–390.
- <sup>51</sup>M. S. P. Lucas, *J. Appl. Phys.* **36**, 1632 (1965).
- <sup>52</sup>R. E. Camley and J. Barnaś, *Phys. Rev. Lett.* **63**, 664 (1989).
- <sup>53</sup>J. Barnaś, A. Fuss, R. E. Camley, P. Grünberg, and W. Zinn, *Phys. Rev. B* **42**, 8110 (1990).
- <sup>54</sup> $\rho$  and  $\ell$  must be understood here as referring to the resistivity and mean free path of the same material as the ultrathin layer under description but with the electrical properties it would have if its thickness would be infinite.
- <sup>55</sup>R. Q. Hood and L. M. Falicov, *Phys. Rev. B* **46**, 8287 (1992).
- <sup>56</sup>L. Vila, T. Kimura, and Y. Otani, *Phys. Rev. Lett.* **99**, 226604 (2007).
- <sup>57</sup>M. D. Stiles and A. Zangwill, *J. Appl. Phys.* **91**, 6812 (2002).
- <sup>58</sup>H. Hoffmann and J. Vancea, *Thin Solid Films* **85**, 147 (1981).
- <sup>59</sup>B. L. Johnson and R. E. Camley, *Phys. Rev. B* **44**, 9997 (1991).
- <sup>60</sup>P. J. Metaxas, J. P. Jamet, J. Ferré, B. Rodmacq, B. Dieny, and R. L. Stamps, *J. Magn. Magn. Mater.* **320**, 2571 (2008).
- <sup>61</sup>R. A. Hajjar, T. Wu, and M. Mansuripur, *J. Appl. Phys.* **70**, 6041 (1991).
- <sup>62</sup>S. Mangin, D. Ravelosona, J. A. Katine, M. J. Carey, B. D. Terris, and E. E. Fullerton, *Nature Mater.* **5**, 210 (2006).
- <sup>63</sup>M. N. Baibich, J. M. Broto, A. Fert, F. Nguyen Van Dau, F. Petroff, P. Etienne, G. Creuzet, A. Friederich, and J. Chazelas, *Phys. Rev. Lett.* **61**, 2472 (1988).
- <sup>64</sup>K. Vahaplar, A. M. Kalashnikova, A. V. Kimel, D. Hinzke, U. Nowak, R. Chantrell, A. Tsukamoto, A. Itoh, A. Kirilyuk, and T. Rasing, *Phys. Rev. Lett.* **103**, 117201 (2009).